Ultrafast high-energy dynamics of thin spherical shells of light ions in the Coulomb explosion of heteroclusters

Isidore Last and Joshua Jortner
School of Chemistry, Tel Aviv University, Ramat Aviv, Tel Aviv 69978, Israel
(Received 30 November 2004; published 28 June 2005)

Severe deviations from uniform Coulomb explosion can be manifested for extremely ionized molecular heteroclusters, due to kinematic effects. We established unique features of the spatial distribution, energetics, and time-resolved dynamics in Coulomb explosion of multicharged light-heavy heteroclusters, consisting of light, low-charge and heavy, high-charge, ions, e.g., hydroiodic acid $(H^+I^{q_I+})_n$ and its isotopic substituents $(D^+I^{q_I+})_n$ and $(T^+I^{q_I+})_n$, where extreme multielectron ionization in ultraintense laser fields (peak intensity $I=10^{17}-10^{20}$ W cm^{-2}) results in $q_I=25$ at $I=10^{19}$ and $q_I=35$ at $I=10^{20}$ W cm^{-2}. Electrostatic models and simulations, based on the cluster vertical ionization (CVI) initial conditions for Coulomb explosion of $(D^+I^{q_I+})_{2171}$ and $(H^+I^{q_I+})_{2171}$ ions with $q_I=25$ (corresponding to $I=10^{19}$ W cm^{-2}), reveal expanding, thin, two-dimensional spherical shells of the light D^+ or H^+ ions, with the monolayer expansion occurring on the femtosecond time scale. Under initial CVI conditions the model and the simulation results for the formation of femtosecond expanding nanoshells of light ions were confirmed by complete simulations involving both electron and nuclear dynamics in $(HI)_{2171}$ and $(DI)_{2171}$ clusters subjected to a Gaussian laser pulse with $I=10^{19}$ W cm^{-2}. The energetic data for the light ions reveal high energies with a narrow energy distribution, e.g., average energy $E_{av}=23$ keV at width $\Delta E/E_{av}=0.16$ for Coulomb explosion of $(D^+I^{q_I+})_{2171}$ clusters. These dynamic, structural and energetic data for light–heavy $(A^+I^{q_I+})_n$ heteroclusters ($A=H$, D, and T) arise from kinematic overrun effects of the A^+ ions. Finally, we address the implications of these Coulomb explosion results of $(D^+I^{q_I+})_n$ heteroclusters for *dd* nuclear fusion driven by heterocluster Coulomb explosion, where the extremely charged I^{q_I+} ions serve as most effective energetic and kinematic triggers for driving the expanding D^+ ions.

DOI: 10.1103/PhysRevA.71.063204 PACS number(s): 36.40.Qv, 36.40.Wa, 33.80.Wz

I. INTRODUCTION

Ultrafast femtosecond electron dynamics and nuclear dynamics in large, finite systems, e.g., elemental and molecular clusters such as $(Xe)_n$, $(D_2)_n$, $(D_2O)_n$, or $(CD_4)_n$, are triggered by their interaction with ultraintense laser fields (peak intensity $I=10^{15}-10^{20}$ W cm^{-2}) [1–9]. Cluster ionization processes are then manifested, with the electron dynamics involving sequential-parallel coupled processes of inner ionization, which results in the formation of a charged energetic nanoplasma within the cluster (or its vicinity), and is followed by (partial or complete) outer ionization of the nanoplasma. Electron dynamics triggers nuclear dynamics, with the outer ionization being accompanied by Coulomb explosion [10–22]. Coulomb explosion is a relatively simple process in the case of cluster vertical ionization (CVI), when the time scales of the inner/outer ionization processes are short compared to the time scale of the ion expansion, and when the outer ionization is complete, i.e., all unbound electrons are removed from the cluster [10–16]. The CVI conditions prevail at high laser intensities ($I=10^{18}-10^{20}$ W cm^{-2}). At the onset of the CVI initial conditions, cluster Coulomb explosion can be considered as a system consisting only of ions, which are initially located at the same geometry as the atoms in the neutral clusters [17]. For the interionic interaction, only repulsive ion–ion Coulomb forces are of importance. Furthermore, the direct effect of the laser field on ion motion is negligibly small, up to $I=10^{20}$ W cm^{-2} [16]. This situation significantly simplifies the theoretical treatment of Coulomb explosion.

The traditional view of Coulomb explosion following extreme cluster multielectron ionization involves uniform ion expansion [16]. Indeed, such uniform expansion prevails for the simplest process of Coulomb explosion of homonuclear molecular $(A^{q_A+})_n$ clusters, with initially uniform, constant charge, and spherically symmetric ion distributions [16]. This initial ion distribution is then characterized by an atomic density $\rho(r_0)=\rho_0$ for $r_0 \leqslant R_0$ and $\rho(r_0)=0$ for $r_0 > R_0$, where R_0 is the cluster radius, and by fixed and uniform ion charges $(q_j=q_A, j=1,2,\ldots,n)$. The expansion of ions in these homonuclear clusters retains the uniform ion distribution, being described by the density $\rho(t)$ at $r \leqslant R(t)$, which is independent of r. $R(t)$ is the expanding cluster radius at time t. Uniform Coulomb explosion is, of course, characterized by a single radius of the expanding cluster. The distribution $P(E)$ of the kinetic energy of the product ions is [11,16,18,20–22]:

$$P(E) = (3/2E_M)(E/E_M)^{1/2}; \quad E \leqslant E_M,$$

$$P(E) = 0; \quad E \geqslant E_M, \tag{1}$$

with the maximal energy E_M provided by the periphery $r_0=R_0$ ions:

$$E_M = (4\pi/3)\bar{B}\rho_0 q_A^2 R_0^2. \tag{2}$$

The average energy distribution of Eq. (1) is

$$E_{av} = (3/5)E_M. \tag{2a}$$

In Eq. (2) and in what follows, the lengths r_0, R_0, and $R(t)$ are expressed in Å, the density ρ_0 in Å^{-3}, the ionic charge q_A in e units, the energies E, E_M, and E_{av} in eV, and $\bar{B} = 14.40$ eV Å.

Uniform Coulomb explosion, which, according to Eqs. (1) and (2), is characterized by the energy distribution $P(E) \propto E^{1/2}$ ($E < E_M$) and by $E_{av} \propto R_0^2$, is well obeyed for elemental and molecular homonuclear clusters at sufficiently high laser intensities where the CVI initial conditions nearly prevail [11,16,18–22]. For molecular heteroclusters deviations from uniform Coulomb explosion were recorded. In Coulomb explosion of highly ionized molecular heterocluster, e.g., ionized heavy water $(D_2^+O^{6+})_n$ or ionized deuterated methane $(C^{4+}D_4^+)_n$, the energy distribution of the light D^+ ions showed marked deviations from Eq. (1), peaking at high energies in the vicinity of $E \sim E_M$ [11,19–22]. This was attributed to kinematic effects [11,19,22] on the ion expansion dynamics. In this paper we explore the new and unique features of the spatial distribution, the energetics and the time resolved dynamics of Coulomb explosion of highly ionized molecular heteroclusters $(A_k^{q_A+}B^{q_B+})_n$, which consist of light A^{q_A+} ions and heavy B^{q_B+} ions, e.g., hydroiodic acid clusters $(H^+I^{q_I+})$ or its isotopic substitutes $(D^+I^{q_I+})_n$ and $(T^+I^{q_I+})_n$. These will be referred to as light–heavy heteroclusters. Severe deviations from uniform Coulomb explosion will be demonstrated in such heteroclusters. Extreme multielectron ionization levels, estimated from the barrier suppression ionization (BSI) model [14] applied to DI and *HI* single molecules, exhibit high positive iodide ion charges, e.g., from $q_I = 7$ at $I = 6 \times 10^{15}$, $q_I = 25$ at $I = 10^{19}$ W cm^{-2}, up to $q_I = 35$ at $I = 10^{20}$ W cm^{-2} [23]. Extreme multielectron ionization levels of $(DI)_n$ heteroclusters ($n = 55$–4213) reported herein will provide the basis for the exploration of the energetics and dynamics of those light–heavy heteroclusters in ultraintense laser fields. On the basis of electrostatic models and simulations for multicharged $(AI)_n$ heteroclusters, we shall unveil new features of Coulomb explosion of the light A^+ ($A = H$, D, and T) ions, which give rise to mobile, radial boundary spherical monoionic shells, expanding on the femtosecond time scale.

In the Coulomb explosion of heteroclusters, overrun processes originating from kinematic effects [19–22] are of major importance. Invoking the CVI initial conditions we consider Coulomb explosion of light–heavy $(A_k^{q_A+}B^{q_B+})_n$ heteroclusters, which consist of light A^{q_A+} ions with mass m_A and heavy B^{q_B+} ions with mass m_B, where $m_A \ll m_B$. The dynamics of the ion expansion is determined by the kinematic parameter [19–22]:

$$\eta_{AB} = q_A m_B / q_B m_A. \tag{3}$$

Typical values for η_{AB} for $(A^+I^{25+})_n$ clusters are $\eta_{HI} = 5.1$ for H^+, $\eta_{DI} = 2.5$ for D^+, and $\eta_{TI} = 1.7$ for T^+. When $\eta_{AB} > 1$, the light A ions overrun the heavy B ions during the Coulomb expansion process [19–22,24,25]. A typical demonstration of the overrun process for heteroclusters consisting of light and heavy ions is presented for simulations of nuclear and electron dynamics of Coulomb explosion of $(C^{4+}D_4^+)_n$ and $(C^{4+}H_4^+)_n$ clusters. Two distinct radii for the expansion of the light (H^+ or D^+) subcluster ions (R_H or R_D) and for the expansion of the heavy C^{4+} subcluster ions (R_C) are exhibited, where $R_H(t)$, $R_D(t) > R_C(t)$ at each t (Fig. 1). The formation of two distinct radii in the Coulomb explosion of these heteroclusters is qualitatively different from the case of homogeneous expansion of a charged homocluster. Also, we shall subsequently show that for $\eta_{AB} \gg 1$ the overrun process results in the contraction of the spatial distribution and in a narrow energy distribution of the expanding light ions. Coulomb explosion of these heteroclusters produces energetic A^{q_A+} ions, in particular deuterons (D^+), with a considerably higher kinetic energy than D^+ from Coulomb explosion of homonuclear $(D_2)_{n/2}$ clusters of the same size [11,19–22]. The advantage of the use of heteronuclear deuterium containing clusters for dd nuclear fusion driven by Coulomb explosion (NFDCE) was theoretically advanced [19–22] and experimentally confirmed for NFDCE of $(CD_4)_n$ clusters [6,9]. For exploding light–heavy heteroclusters, e.g., $(DI)_n$ or $(CD_3I)_n$ in ultraintense laser fields, the extremely charged I^{q+} ($q = 7$–35) ions will act as most effective energetic triggers for driving the D^+ ions to high energies, leading to a marked enhancement of the NFDCE yield.

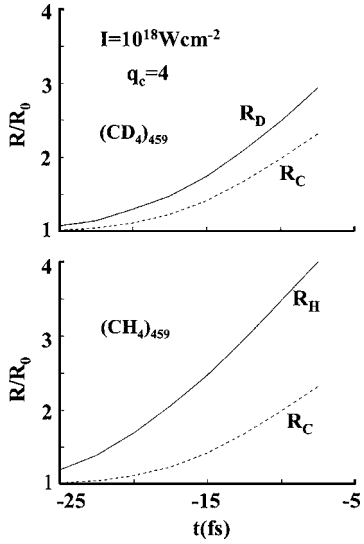

FIG. 1. Femtosecond time dependence of the radii $R_C(t)$ and $R_D(t)$ and of the radii $R_C(t)$ and $R_H(t)$ for Coulomb explosion of $(C^{4+}D_4^+)_{459}$ and of $(C^{4+}H_4^+)_{459}$ clusters, respectively. The values of the radii $r_\alpha(t)$ ($\alpha = C$, D, and H) are normalized to the corresponding initial value $R_\alpha(0)$. The radial distributions of the heavy (C^{4+}) and the light (D^+ or H^+) ions are different at each time, with the corresponding radii being given by their spatial limits (Ref. [16]). In the expansion of these multicharged heteroclusters [with the kinematic parameters, Eq. (3), $\eta_{CH} = 3.0$ and $\eta_{CD} = 1.5$] an overrun effect of the light H^+ and D^+ ions relative to the heavy C^{4+} ions is exhibited, with $R_H(t)$, $R_D(t) > R_C(t)$ at each t. Data were obtained from $E+N$ simulations involving both electron and nuclear cluster dynamics (Refs. [14–16,22]) induced by a Gaussian pulse with a pulse width of $\tau = 25$ fs, a peak intensity of $I = 10^{18}$ W cm^{-2}, and a temporal pulse onset at $t_S = -30$ fs.

II. METHODOLOGY OF SIMULATIONS OF COULOMB EXPLOSION DRIVEN BY EXTREME MULTIELECTRON IONIZATION OF MOLECULAR HETEROCLUSTERS

The energetics and dynamics of Coulomb explosion of multicharged $(AI)_n$ heteroclusters ($A=H$, D, and T) were explored by electrostatic models (Sec. IV) and by simulations. Two simulation methods were adopted herein:

A. Coulomb explosion under initial CVI conditions of ionic $(A^+I^{q_I+})_n$ heteroclusters ($A=H$, D, and T)

Molecular dynamics simulations (based on trajectories of the ions) were performed for $q_I=25$, as appropriate for extreme multielectron ionization at $I=10^{19}$ W cm^{-2} (see point (B) above). The initial structure for ionic clusters was taken as that of the corresponding neutral $(AI)_{2171}$ heterocluster, as appropriate for the CVI model.

B. Complete simulations including both high-energy electron and nuclear dynamics in an ultraintense laser field (Refs. [14–16,22])

These simulations for the dynamics of the charged constituents, together with the laser–matter interactions will be referred to as $E+N$ simulations. These $E+N$ simulations include electron dynamics processes of inner ionization, nanoplasma formation and outer ionization, and of nuclear dynamics processes induced by a (Gaussian) laser pulse [14–16,22]. The laser field is

$$F_\ell(t) = F_{\ell 0}(t)\cos(2\pi\nu t + \phi_0), \tag{4}$$

(for $-\infty \leqslant t \leqslant \infty$), with the frequency $\nu=0.35$ fs^{-1} (photon energy 1.44 eV) and phase $\phi_0=0$, where $F_{\ell 0}(t)$ is the laser field envelope:

$$F_{\ell 0}(t) = F_M \exp[-2.773(t/\tau)^2], \tag{4a}$$

where F_M is the maximal electric field (which is related to the laser peak intensity by $(e|F_M|=2.75\times 10^{-7}\ I^{1/2}$ eV Å^{-1}), and τ (=25 fs) is the pulse temporal width. The laser field [Eqs. (4) and (4a)], is defined in the temporal range $t>-\infty$, and the peak of the laser pulse is attained at $t=0$. An initially truncated Gaussian pulse was used in the $E+N$ simulations, with the initial laser field $F_\ell=F_s$ being located at $t=t_s<0$. We took [14] $F_s=(F^{th}+F^{co})/2$, where F^{th} is the threshold laser field for the first single electron ionization of each molecule, while F^{co} is the laser field for complete one-electron ionization of all the constituent atoms within the molecular cluster [i.e., for $(DI)_n$ the complete one-electron ionization level is 2, with $eF^{th}=2.5$ eV Å^{-1}, $eF^{co}=2.9$ eV Å^{-1} and $eF_s=2.7$ eV Å^{-1}]. At the initial laser field F_s at $t=t_s$, all the cluster atoms are taken as singly charged ions, with the electrons being located at the BSI distance [14]. The cluster inner field ionization, which is driven by a composite field consisting of the laser field and the inner field induced by ions +electrons, was described in terms of the BSI for each constituent. An additional, rather small, contribution to the inner ionization [12%, 4%, and 3% for $(DI)_{2171}$ at $I=10^{17}$, 10^{18}, and 10^{19} W cm^{-2}, respectively] results from electron impact ionization [14]. Molecular dynamics simulations, based on the trajectories of the energetic electrons and of the ions, were performed by molecular dynamics simulations, incorporating electron–electron, electron–ion, ion–ion, and electron/ion–laser interactions. High-energy electron dynamics (at $I>10^{18}$ W cm^{-2}) incorporated relativistic effects and were subjected to magnetic effects for electron–laser interactions [14,15].

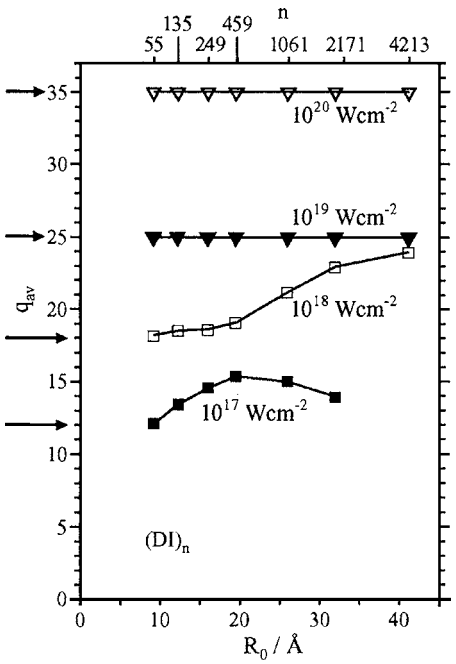

FIG. 2. $E+N$ simulations of the cluster size and laser intensity dependence of the average inner ionization level (q_{av}) for I^{q_I+} ions in $(DI)_n$ heteroclusters ($n=55-4342$). The laser intensities are marked on the curves. The ionization levels of the single DI molecule at these intensities, calculated by the BSI model [with ionization potentials taken from Th. A. Carlson, C. W. Nesta, N. Wasserman, and J. D. McDowel, At. Data **2**, 63 (1970)], are marked by horizontal arrows.

The ionization level of $(DI)_n$ heteroclusters obtained from $E+N$ simulations is characterized by the average charge q_{av} $(=\langle q_I\rangle)$ on each iodine ion. In Fig. 2 we portray the cluster size dependence of the ionization level of $(DI)_n$ heteroclusters ($n=55-4213$) in the intensity range $I=10^{17}-10^{20}$ W cm^{-2}. In Fig. 2 we also present the comparison between the extreme multielectron ionization levels of the single DI molecule [23] (marked by horizontal arrows) and of the cluster. In the intensity domain of $I=10^{17}-10^{18}$ W cm^{-2}, the single molecule extreme multielectron ionization level constitutes a lower limit for the multielectron ionization level of the cluster (Fig. 2). For the intensity of $I=10^{18}$ W cm^{-2}, q_{av} increases from the single molecule value for small clusters, i.e., $(DI)_{55}$, to higher values with increasing the cluster size (Fig. 2), where ignition effect [14,15] lead to the enhancement of q_{av} for larger clusters. For a somewhat lower intensity of $I=10^{17}$ W cm^{-2}, q_{av} first increases from the single molecule value and subsequently decreases with increasing the cluster size (Fig. 2). This composite behavior reflects the interplay between igni-

tion effects and nanoplasma screening effects [14,15]. In the intensity range of $I=10^{17}-10^{18}$ W cm^{-2}, a distribution of q_I values [as demonstrated in detail for Xe_n clusters [15], which are isoelectronic with $(HI)_n$] is excited. In the highest intensity domain of $I=10^{19}-10^{20}$ W cm^{-2}, the iodine atom charges on the individual molecules within the cluster are cluster size independent, being identical to the q_I values for a single molecule (Fig. 2). Furthermore, a single ionic charge is observed in this intensity range, i.e., $q_I=25$ for $I=10^{19}$ W cm^{-2} and $q_I=35$ for $I=10^{20}$ W cm^{-2}. In this highest intensity domain the strength of the laser–ion interactions dominates over electrostatic interactions within the cluster, resulting in a cluster size independent ionization level and a (nearly) delta function distribution of the ionic charges q_I (i.e., $q_I=q_{av}$). Furthermore, for Gaussian pulses in this highest intensity domain, the CVI initial conditions are nearly obeyed [16]. Led by these guidelines, we performed ordinary molecular dynamics simulations for Coulomb explosion of $(D^+I^{25+})_n$ clusters under CVI initial conditions [section (A)] and confronted these data with the results for $E+N$ simulations [section (B)] for $(DI)_n$ clusters at $I=10^{19}$ W cm^{-2}.

III. ENERGETICS OF COULOMB EXPLOSION OF LIGHT–HEAVY HETEROCLUSTERS

Within the framework of the CVI, we consider the extreme case of Coulomb explosion of a light–heavy $(A_k^{q_A+}B^{q_B+})_n$ cluster with light A^{q_A+} ions ($m_A \ll m_B$), with $q_A=1$ (for $A \equiv H$, D, or T). For these heteroclusters we take $kq_A \ll q_B$ and $\eta_{AB} \gg 1$. The first condition enables us to ignore the light ion charge and the second condition enables us to ignore the heavy ion motion during the time scale of the light ion motion through the B^{q_B+} ion subcluster (the B core), whereupon Coulomb explosion is dominated by the motion of light ions. In the framework of these approximations simple electrostatic considerations provide the following potential for an A^{q_A+} ion:

$$U(r) = (2\pi/3)\bar{B}\rho_0 q_B q_A (3R_0^2 - r^2), \quad r \leqslant R_0, \tag{5}$$

$$U(r) = (4\pi/3)\bar{B}\rho_0 q_B q_A R_0^3/r, \quad r > R_0. \tag{5a}$$

The final kinetic energy $E(r_0)$ of an A ion initially located at $r_0 \leqslant R_0$, where R_0 is the initial heterocluster radius, is equal to $U(r_0)$, being given by

$$E(r_0) = (1/2)(3 - (r_0/R_0)^2)E_{\min}, \tag{6}$$

where

$$E_{\min} = (4\pi/3)\bar{B}\rho_0 q_B q_A R_0^2. \tag{6a}$$

The A^{q_A+} ions from the inner region of the cluster, $r_0 < R_0$, pass the initial cluster border R_0 with some kinetic energy gaining larger final energy than the periphery A^{q_A+} ions, $r_0=R_0$. Consequently, the periphery A ions provide a minimal energy, in contrast to the case of homonuclear clusters, Eqs. (1) and (2). The energy distribution of the final energies of the light ions is derived from Eq. (6) in the form

$$P(E) = (3/E_{\min})[3 - 2(E/E_{\min})]^{1/2}; \quad E_{\min} \leqslant E \leqslant \frac{3}{2}E_{\min}, \tag{7}$$

and the average energy is

$$E_{av} = (6/5)E_{\min}. \tag{7a}$$

The average kinetic energy, Eq. (7a), and the kinetic energy distribution, Eq. (7), for Coulomb explosion of the light-heavy heterocluster quantitatively differ from the energetics of Coulomb explosion of homonuclear clusters, Eqs. (1) and (2). Several qualitative and quantitative differences should be noted.

(1) The energy distribution for the light ions from the heterocluster is characterized by a finite minimal energy $E_{\min}$, and a maximum energy of $3E_{\min}/2$. The distribution, Eq. (7), as distinct from the energy distribution of the ions of the homonuclear cluster, Eq. (2), is characterized by the lower limit of $E_{\min}$.

(2) The dependence of both $E_{\min}$, Eq. (6a), and of E_M, Eq. (2), on the parameters of the exploding ionic clusters is similar, both scaling with R_0^2, while for the heterocluster $E_{\min} \propto q_A q_B$ and for the homocluster $E_M \propto q_A^2$. As $q_A \ll q_B$, the lowest energies of the A ions exploding from the heterocluster are considerably higher than the highest energies of the A ions from the homocluster.

(3) The energy distribution for Coulomb explosion from the heterocluster, Eq. (7), is relatively narrow, being (5/12) E_{av} (corresponding to 42% of E_{av}). On the other hand, the energy distribution for Coulomb explosion of the homonuclear cluster is considerably broader, being $E_M \simeq (5/3)E_{av}$ (corresponding to 166% of E_{av}).

(4) The average energy of the A ions for Coulomb explosion of the heterocluster, Eq. (7a), is $E_{av}=(6/5)E_{\min}$, while the average energy for the homonuclear cluster, Eq. (2a), is $E_{av}=(3/5)E_M$. Both average energies scale as R_0^2. As $E_{\min}/E_M = q_B q_A \gg 1$ [point (2) above], we expect that the average energy for Coulomb explosion of the light ion heterocluster will be enhanced relative to that of the ions from the homonuclear cluster of the same size, manifesting the effects of energetic triggering, which is important for NFDCE.

Simulations of Coulomb explosion with CVI initial conditions were performed for the ionic $(A^+I^{25+})_{2171}$ heteroclusters ($A=H$, D, and T). The simulation results (Fig. 3) show a low energy onset around $E_{\min}=23$ keV, which is somewhat higher than the value of $E_{\min}=21$ keV calculated from Eq. (6a). The simulation results confirm the narrow shape of the energy distribution predicted by Eq. (7). In contrast to the theoretical model, Eq. (7), the CVI simulations reveal an isotope effect (Fig. 3). The difference between the predictions of the electrostatic model and the simulation results originate from the (slow) motion of the heavy ions in the latter case. Distinct from the theoretical distribution, Eq. (7), the simulation results demonstrate the existence of a low energy "tail" (Fig. 3), generated most probably by the A ion collisions with the B ions. The "tail" contribution increases with decreasing the kinematic parameter η_{AI} with the increase of the ion mass in the sequence H^+, D^+, and T^+. The

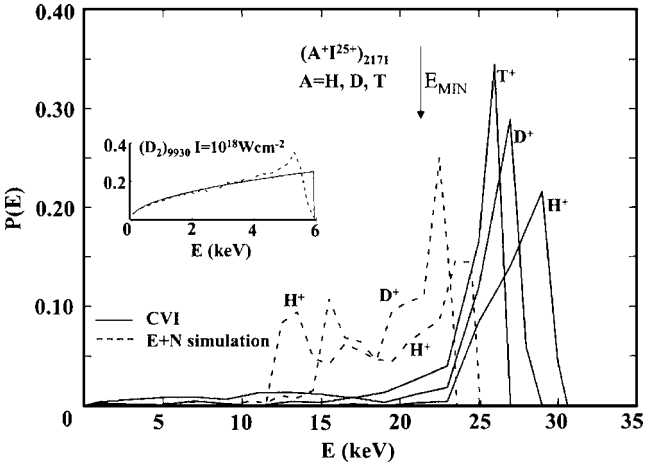

FIG. 3. Energetics of Coulomb explosion of extremely multicharged hydroiodic acid and its isotopic species. The solid curves represent molecular dynamics simulations of the kinetic energy distributions $P(E)$ of A^+ ions from Coulomb explosion of $(A^+I^{25+})_{2171}$ heteroclusters ($A=H$, D, or T) under CVI initial conditions. The dashed curves represent kinetic energy distributions obtained from $E+N$ simulations including both electron inner/outer ionization dynamics and nuclear dynamics in $(AI)_{2171}$ heteroclusters subjected to a Gaussian laser field with $I=10^{19}$ W cm^{-2} and $\tau=25$ fs, using the procedure of Refs. [14–16,22]. The curves marked H^+, D^+, and T^+ represent data for the three isotopes. $E_{\min}$ marks the low energy onset, Eq. (6a). For the sake of comparison, the inset shows the kinetic energy distribution obtained from $E+N$ simulations of the kinetic energy distribution of D^+ ions from Coulomb explosion of $(D_2)_{9930}$ homonuclear clusters in a laser field of $I=10^{18}$ W cm^{-2} (Ref. [16]), with the dashed line representing the simulation results, while the solid line corresponds to Eqs. (1)–(3).

energy distribution interval, ΔE, which includes 75% of the ions, is impressively narrow, corresponding to $\Delta E=0.14E_{av}$, $0.13E_{av}$, and $0.16E_{av}$ for H^+, D^+, and T^+ ions, respectively. These simulated values of ΔE are lower than the value of $\Delta E=0.25E_{av}$ obtained from the theoretical distribution, Eq. (7). Together with the CVI energy distributions, in Fig. 3 we also show the energy distribution obtained by complete $E+N$ simulations for $(DI)_{2171}$ and $(HI)_{2171}$ clusters subjected to a Gaussian shaped laser pulse with a peak intensity of 10^{19} W cm^{-2} (Sec. II). On the basis of the results and analysis of the cluster multielectron ionization levels presented in Sec. II, we inferred that the use of the constant charge $q_I=25$ in the CVI simulations is justified on the basis of the $E+N$ simulations for $I=10^{19}$ W cm^{-2}. The D^+ ion energy obtained by $E+N$ simulations, $E_{av}=19.5$ keV, is smaller than the CVI energy of $E_{av}=25.5$ keV, the decrease being due to the coupling between outer ionization electron dynamics and Coulomb explosion nuclear dynamics induced by the Gaussian pulse [16]. The energy distribution provided by the $E+N$ simulations shows two peaks in $P(E)$, which is somewhat wider than in the case of CVI simulations (Fig. 3), due to finite-time outer ionization effects [15,16]. The width of this energy distribution is, however, still relatively narrow, being $\Delta E=0.33\ E_{av}$. The last issue we would like to address in this context is the role of electron dynamics involving inner and outer ionization on the nuclear dynamics of Coulomb explosion [15,16,22]. Similar $E+N$ simulations were also performed for inner/outer ionization and Coulomb explosion of $(CD_3I)_{2171}$ [26] and $(CD_4)_{2171}$ [22] clusters, using the same laser pulse as used herein for the $(DI)_{2171}$ cluster. The energy distribution widths of D^+ ions for Coulomb explosion of $(CD_3I)_{2171}$ and of $(CD_4)_{2171}$ clusters are $\Delta E=0.27E_{av}$ and $\Delta E=0.24E_{av}$, respectively [22,26]. Accordingly, the narrow energy distribution of light (D^+ or H^+) ions from Coulomb explosion of light–heavy heteroclusters is universal.

The results obtained by us show that at higher laser intensities, when the CVI or pseudo-CVI [16] conditions are fulfilled, the energy of $A^{q_{A^+}}$ ions produced from a single heteronuclear $(BA_k)_n$ cluster is characterized by a narrow spread around the average energy E_{av}. The average energy is, however, strongly cluster size dependent, increasing as R_0^2, Eqs. (6a) and (7a). This pattern of a narrow kinetic energy distribution of the light ions in the Coulomb explosion of multicharged light–heavy heteroclusters (Fig. 3), qualitatively and quantitatively differs from the broad energy distribution in Coulomb explosion of homonuclear clusters, which is described by Eqs. (1)–(3) (inset to Fig. 3). It appears that the widespread ion energy observed in Coulomb explosion experiments with heteronuclear clusters [9,27] is due to the spread in the cluster sizes, which is usually wide [9,28,29] but is not due to the narrow energy spread provided by single clusters.

IV. TIME-RESOLVED ULTRAFAST DYNAMICS OF COULOMB EXPLOSION OF LIGHT–HEAVY HETEROCLUSTERS

We now consider the time-resolved distribution and the dynamics of the light $A^{q_{A^+}}$ ions from Coulomb explosion of the light–heavy $(A_k^{q_{A^+}}B^{q_{B^+}})_n$ heteroclusters. We shall again apply the electrostatic model with a static configuration of the heavy ions. The expansion time $t(r;r_0)$ of a light ion initially located at radius $r_0(<R_0)$ to reach radius r can be expressed by the integral of the reciprocal velocity of the light ion (relative to the center of mass) $v(r';r_0)$ at r' $(r_0 \leqslant r' \leqslant r)$, expressed in the form [17,30]:

$$t(r;r_0)=\int_{r_0}^{R_0} dr'/v(r';r_0). \tag{8}$$

This classical expression, Eq. (8), was used by Bersohn and Zewail [30] to describe ultrafast dissociation dynamics of ICN and was adopted for Coulomb explosion dynamics [17,31]. The velocity can be expressed in terms of the ion kinetic energy $E(r';r_0)$ at r':

$$v(r';r_0)=[2E(r';r_0)/m_A]^{1/2}. \tag{8a}$$

The time $t(r;r_0)$ for an ion initially located at $r_0(\leqslant R_0)$ to reach the radius $r(\geqslant R_0)$, Eq. (8), is

$$t(r;r_0)=t(R_0;r_0)+t(r;R_0), \tag{9}$$

where the time for the ion motion from r_0 to the B core border R_0 is

$$t(R_0;r_0) = \int_{r_0}^{R_0} dr'/[2E(r';r_0)/m_A]^{1/2}. \quad (10)$$

The kinetic energy at $r<R_0$ is

$$E(r;R_0) = (E_{\min}/2)(\hat{\xi}^2 - \hat{\xi}_0^2); \quad \hat{\xi}_0 \leqslant \hat{\xi} \leqslant 1, \quad (11)$$

with

$$\hat{\xi} = r/R_0$$

$$\hat{\xi}_0 = r_0/R_0, \quad (11a)$$

and $E_{\min}$ is given by Eq. (6a).

Outside the B core, the time $t(r;R_0)$ for the ion motion from R_0 to $r(r>R_0)$ is given by Eqs. (8) and (8a). The ion energy, according to Eqs. (5) and (5a), is given by

$$E(r;r_0) = E_{\min}[(3/2) - (\hat{\xi}_0^2/2) - \xi], \quad (12)$$

with

$$\xi = R_0/r; \quad \xi < 1. \quad (12a)$$

Equations (9)–(12) result in the Coulomb explosion time of the light ions:

$$t(r;r_0) = t_0\tau(\hat{\xi}_0,\xi) \quad (13)$$

whose time constant t_0 is

$$t_0 = C(m_A/\rho_0 q_A q_B)^{1/2} \quad (14)$$

with $C=0.930$ fs Å$^{-3/2}$, and the reduced time $\tau(\hat{\xi}_0,\xi)$ is

$$\tau(\hat{\xi}_0,\xi) = \ell n\{[1+(1-\hat{\xi}_0^2)^{1/2}]/\hat{\xi}_0\} + \varphi^{3/2}[Z(\varphi\xi) - Z(\varphi)], \quad (15)$$

where

$$\varphi = 2[3-\hat{\xi}_0^2]^{-1} \quad (16)$$

and $Z(x)$ is the Coulomb expansion function [31]:

$$Z(x) = (1-x)^{1/2}/x + (1/2)\ell n\{[1+(1-x)^{1/2}]/[1-(1-x)^{1/2}]\}. \quad (17)$$

The dependence of the expansion distance r/R_0 on the initial distance r_0/R_0 (in reduced units) calculated from Eq. (13) enables us to construct the histograms of the time-dependent radial distribution $P(r)$ of the light ions, which are portrayed in Fig. 4 for the reduced times $\tau(\hat{\xi},\xi_0)$, Eq. (15). In Fig. 5 we present the predictions of the electrostatic model for the arrival distances r of the light ions calculated for fixed values of $\tau(\hat{\xi},\xi_0)$. Light ions arrive at the same final distance r from two different initial r_0 radii (Fig. 5), manifesting the overrun process which induces the transformation of the initially formed uniform sphere of $A^{q_{A^+}}$ ions into an expanding narrow shell. At the point where $dr/dr_0=0$ (Fig. 4), the light ion distribution diverges, manifesting the sharp spikes in $P(r)$ (Fig. 5), where the narrow distribution peaks at a large, but finite, value, because of the finite r_0 steps used in the numerical calculations based on Eq. (13). The peak of the narrow distribution $P(r/R_0)$ at $r=r_M$ marks the radius of the expanding shell of the light ions. r_M/R_0 increases nearly linearly with increasing τ (inset to Fig. 4) as appropriate for the uniform expansion of the thin spherical shell.

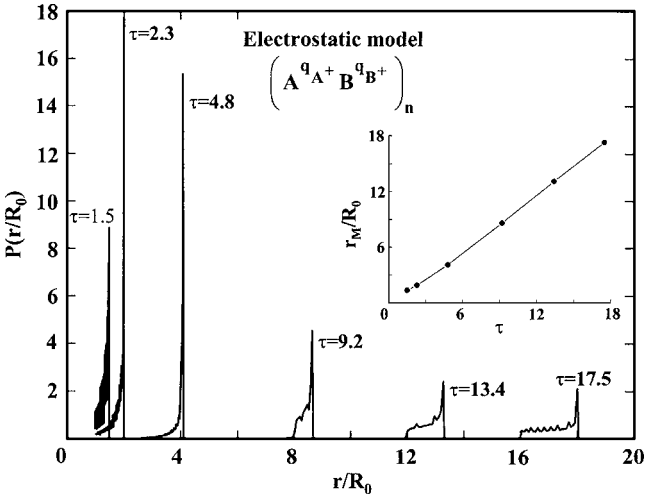

FIG. 4. Application of the electrostatic model (Chap. 4) for Coulomb explosion of light–heavy multicharged $(A_n^{q_{A^+}}B^{q_{B^+}})_n$ heteroclusters. Histograms of the lifetime dependent radial distribution $P(r/R_0)$ [or $P(\xi)$] of the light $A^{q_{A^+}}$ ions with fixed times $\tau(\hat{\xi}_0,\xi)$, Eq. (15), (marked as τ on the curves) were calculated from Eq. (13). The narrow, sharp distributions peak at a value of $r=r_M$. The inset shows the dependence of r_M/R_0 on τ, which is linear for $\tau>2$ and $r_M/R_0>2$.

The results for the expanding soft narrow shell of light ions, which were obtained by the electrostatic model (Figs. 4 and 5), are supported by molecular dynamics simulations of

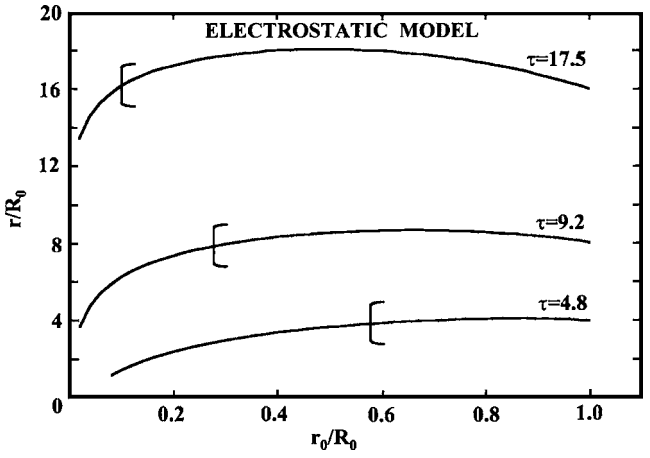

FIG. 5. Features of the electrostatic model for Coulomb explosion of light–heavy multicharged heteroclusters r/R_0 on the initial r_0/R_0 distance of the light ions, Eq. (11a), for several times $\tau(\hat{\xi}_0,\xi)$, Eq. (15), (marked as τ on the curves). Note that light ions arrive at the same final distance from two different initial r_0 radii with the vertical short lines marking the lower limits r_0/R_0 for the attainment of this overrun process, which induces the formation of an expanding narrow shell. At the maxima of the curves ($dr/dr_0=0$) the light ion distribution diverges, manifesting the spikes in the $P(r)$ curves of Fig. 4.

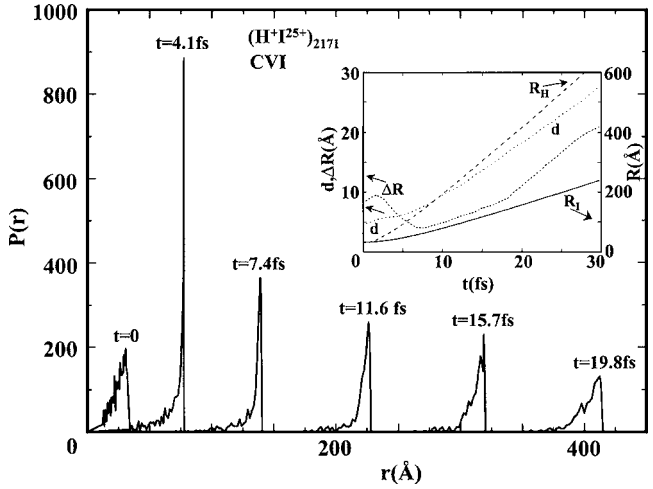

FIG. 6. Molecular dynamics simulations under CVI initial conditions of Coulomb explosion of $(H^+I^{25+})_{2171}$ heteroclusters, representing the ultrafast (fs) time dependence of the spatial distribution $P(r)$ of the H^+ ions at the times marked on the curves. The inset shows the time dependence of the distribution of the H^+ ions (R_H) and of the I^{25+} ions (R_I), the distribution width ΔR and the average interionic distance between the H^+ ions.

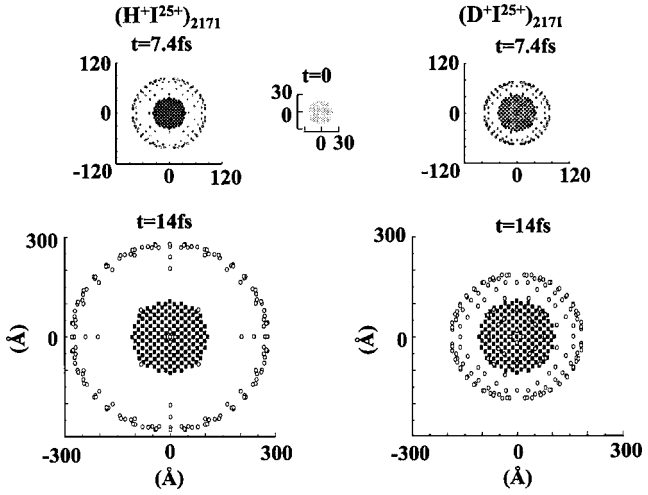

FIG. 8. Two-dimensional images of the spatial configuration of Coulomb expanding $(H^+I^{25+})_{2171}$ and $(D^+I^{25+})_{2171}$ light-heavy heteroclusters under CVI initial conditions at $t=0$, 7.4 and 14 fs. Black squares (■) represent I^{25+} ions, while circles (○) represent light H^+ or D^+ ions. This pictorial presentation reveals the formation of narrow expanding shells of light H^+ and D^+ ions, together with an isotope effect in the expansion dynamics of the shell.

ion expansion. These simulations were performed for nuclear dynamics under initial CVI conditions. In contrast to the electrostatic model, these simulations take into account the interactions between all ions and the motion of all ions, not only the A ions. The CVI simulations were performed for the $(H^+I^{25+})_{2171}$ (Fig. 6) and the $(D^+I^{25+})_{2171}$ clusters (Fig. 7), where we portray the radial distributions $P(r)$ for the light H^+ and D^+ ions. Some quantitative features of Coulomb explosion and of the expansion of both light and heavy ions are presented in the insets to Figs. 6 and 7. In accordance with the predictions of the electrostatic model, the simulations

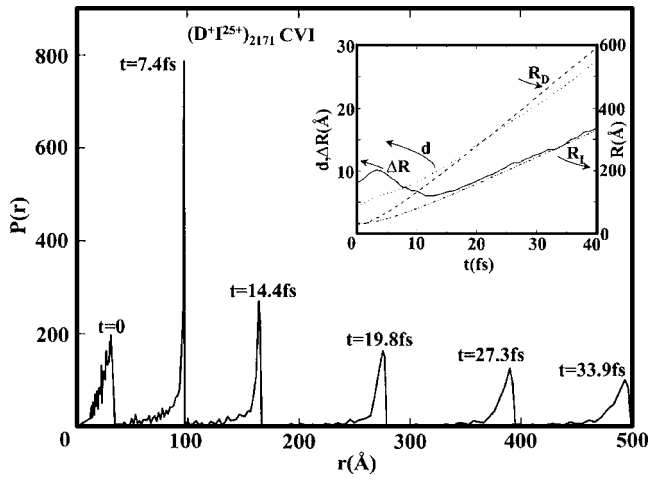

FIG. 7. Molecular dynamics simulations under CVI initial conditions of Coulomb explosion of $(D^+I^{25+})_{2171}$ heteroclusters, representing the ultrafast (fs) time dependence of the spatial distribution $P(r)$ of the D^+ ions at the times marked on the curves. The inset shows the time dependence of the mean radii of the distribution of the D^+ ions (R_D) and of the I^{25+} ions (R_I), the distribution width ΔR and the average interionic distance d between the D^+ ions.

demonstrate the formation of narrow shells of expanding light ions, pictorially represented in Fig. 8.

The following results of the simulations under CVI initial conditions (Figs. 6–8) are notable:

(1) Narrow expanding shells of light H^+ and D^+ ions are manifested (Figs. 6–8).

(2) Soon after the onset of Coulomb explosion (t_ν =4.1 fs for H^+ and t_ν=7.4 fs for D^+ ions), the expanding shells of the light atoms become very narrow (Figs. 6 and 7). The initial times t_ν for narrow shells manifest a normal isotope effect, roughly of the form $\sim m_A^{1/2}$ (insets to Figs. 6 and 7).

(3) The shape of these narrow expanding shells does not considerably depend on the mass of the light ions (Figs. 6 and 7).

(4) The expansion times for the narrow shells at $t>t_\nu$ manifest an isotope effect, which depends on $m_A^{1/2}$ (insets to Figs. 6–8).

(5) At $t>t_\nu$ the shells slowly begin to broaden, with the shell structure of Coulomb explosion being preserved (Figs. 6 and 7).

Quantification of the features of the expanding narrow shells is portrayed in the inset to Fig. 6 for $(H^+I^{25+})_{2171}$ and in the inset to Fig. 7 for (D^+I^{25+}) where we present the mean radii R_H and R_D of the fast expanding light H^+ and D^+ ions, respectively, the mean radius R_I of the slowly expanding heavy I^{25+} ions, the width ΔR of the shells of the H^+ and D^+ ions, and the mean distance d between the light ions. The shell widths ΔR [defined as the $P(r)$ domain around the maximum $P(r)$ containing 50% of the light ions] first slightly increase, but soon start to decrease, reaching a minimum (4 Å for H^+ shells at $\bar{t}$=7 fs, and 5 Å for D^+ shells at $\bar{t}$ =12 fs), and subsequently start to increase at longer times, being nearly proportional to the shell radius with ΔR remaining narrow. The simulation results reveal that $(\Delta R/R)_H$

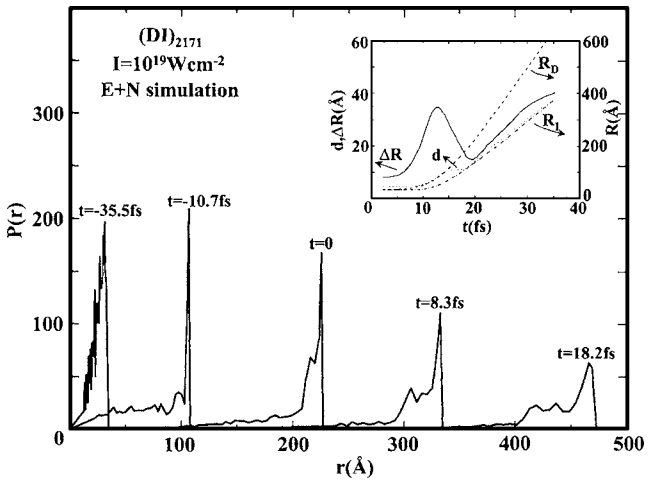

FIG. 9. $E+N$ simulations of Coulomb explosion in $(DI)_{2171}$ heteroclusters subjected to a Gaussian laser field with peak intensity $I=10^{19}$ W cm^{-2}, pulse width $\tau=25$ fs and temporal pulse onset at $t_s=-35.5$ fs. The curves present the spatial distributions $P(r)$ at times t, marked on the curves, with the first curve obtained at $t=t_s$. The inset shows the values of R_D, R_I, ΔR, and d, as defined in Fig. 7.

$\simeq 0.022$ and $(\Delta R/R)_D \simeq 0.027$, so that the relatively narrow shell structure is preserved (insets to Figs. 6 and 7). The average interionic distance d at $t \lesssim \bar{t}$ is lower than ΔR, while d exceeds ΔR at $t > \bar{t}$. At these longer times $d > \Delta R$ (insets to Figs. 6 and 7), providing a two-dimensional monolayer expansion. The smooth increase of the average interionic distance d with time, together with the two-dimensional nature of the expansion, precludes any shock phenomena previously proposed for Coulomb explosion of homonuclear charged clusters with a decreasing density profile.[32]

The simulations under initial CVI conditions, together with the predictions of the analytical model, confirm the formation of expanding narrow shells of light ions. The complete $E+N$ simulation (see Sec. II), involving both electron and nuclear dynamics [14–16,22] was applied to a $(DI)_{2171}$ cluster subjected to a Gaussian laser pulse, with the laser peak intensity $I=10^{19}$ W cm^{-2}. As noted in Sec. II, at this intensity the ionization level of the iodine atoms is $q_I=25$, being the same as in our CVI molecular dynamics simulations. The shell structure for the complete simulations for $(DI)_{2171}$ is somewhat broader (by a numerical factor of ~ 2) than the CVI simulation results (Fig. 8), i.e., $(\Delta R/R)_D = 0.06$ in the linear range (inset to Fig. 9), as compared to $(\Delta R/R)_D = 0.027$ for the CVI simulations (Figs. 7 and 9). This difference manifests the role of outer ionization electron dynamics [14,15]. At an advanced stage of the expansion, the shell of the light ions manifests a bimodal distribution (Fig. 9) reflecting the presence of faster ions (higher maximum) and slower ions (lower maximum), which is also exhibited in the energy distribution $P(E)$ in Fig. 3. As distinct from the CVI results, the complete electron and nuclear simulations demonstrate a relatively high maximum of the shell width $\Delta R(t)$ and a weak minimum of the interionic distance $d(t)$ in the vicinity of the $\Delta R(t)$ minimum (inset to Fig. 9). The general character of the ΔR and d time dependence is similar to that of the CVI simulations portrayed in the insets to Figs. 6 and 7. In particular, for longer times in the linear increasing range of ΔR and of d we note that $d > \Delta R$ (inset to Fig. 9), so that the two-dimensional shell structure is preserved.

V. CONCLUDING REMARKS

Simple electrostatic models, together with simulations based on CVI initial conditions and on complete electron and nuclear dynamics for Coulomb explosion of extremely charged light–heavy heteroclusters (with a large kinematic parameter η), reveal mobile, two-dimensional, spherical thin shells of the light ions, which expand on the femtosecond time scale. The energetic data for the light ions reveal high energies with a narrow energy distribution of finite width ΔE, e.g., $E_{av}=23$ keV and $\Delta E/E_{av}=0.16$, for D^+ ions from Coulomb explosion of $(D^+I^{25+})_{2171}$ clusters. It is also worth noting that, while the ionic kinetic energy is not completely monochromatic, the spatial ionic distribution (of H^+ or D^+) is characterized by an exploding multicharged monolayer. These seemingly counterintuitive results are reconciled on the basis of our electrostatic model. These unique dynamic, structural, and energetic data for exploding multicharged heteroclusters arise from kinematic overrun effects.

The formation of two-dimensional spherical shells of light ions that expand on the femtosecond time scale was rationalized in terms of an electrostatic model. The simplest version of the electrostatic model, with a static configuration of the heavy ions, was utilized (Secs. III and IV) for the elucidation of the spatial configuration, nuclear dynamics and energetics of the expanding thin spherical shells of the light ions. From the point of view of methodology, a slight extension of the electrostatic model will provide further insight into the nature of the expansion of this thin two-dimensional sphere (Fig. 8). The potential energy of the thin sphere of radius $R \gg R_0$, with $\Delta R \ll R$, inferred from the extension of the electrostatic model, is $U=U_1+U_2$. Here $U_1=nkE_{\min}R_0/R$ is the light ion–heavy ion potential energy inferred from Eqs. (4a) and (6a), while $U_2=\bar{B}Q^2/R$ is an additional term due to the light ion–light ion potential energy, with $Q=nkq_A$ being the total charge of the sphere. Accordingly we have

$$U=\bar{B}n^2kq_Aq_B/R+\bar{B}(nk)^2q_A^2/R. \tag{18}$$

The first term in Eq. (18) corresponds to the pressure (p)-volume (V) energy term, while the second term corresponds to the surface tension (γ)-surface (s) energy term. The dominating contribution of the pressure-volume term over the surface tension-surface term, i.e., $U_1 \gg U_2$, implies that $kq_A \ll q_B$, in accord with the simplified electrostatic model used in Secs. III and IV. The energy change is

$$dU=-pdV+\gamma ds, \tag{19}$$

where the negative sign for the pdV term represents internal pressure from inside the sphere. The pressure $p=-(\partial U/\partial V)_s$ is given by

$$p=\bar{B}(n^2k/4\pi)q_Aq_B/R^4. \tag{20}$$

The pressure originating from light ion–heavy ion repulsion is proportional to n^2k and to q_Aq_B, and decreases with the

shell radius as R^{-4}. The surface tension $\gamma=(\partial U/\partial s)_v$ is given by

$$\gamma=-\bar{B}(n^2k^2/8\pi)q_A^2/R^3. \tag{21}$$

The surface tension is negative, due to light ion–light ion repulsion. The surface tension is proportional to $(nk)^2$, to q_A^2 and to R^{-3}. The expanding thin spherical shell of light ions is analogous to a "soap bubble" with a negative surface tension driven by Coulomb pressure, due to light ion–heavy ion repulsion.

The large peak value in $P(r)$, together with the narrow shell structure (Figs. 6–9) and, consequently, the large apparent volume density ρ_v, does not imply shock phenomena in these ionic shells. The conditions for shock phenomena, which were previously proposed for Coulomb explosion of homonuclear clusters with a marked density gradient [32] involve a significant decrease in the mean distance between the particles, and are not reflected in our results for Coulomb explosion of light–heavy heteroclusters. In our simulation the mean distance d between the light ions is comparable to the shell with ΔR (insets to Figs. 6 and 7), whereupon the expansion is essentially two-dimensional with the absence of shock wave phenomena. The condition for shock phenomena is the significant decrease in the distance between particles, which can be accomplished only in a three-dimensional system. In a three-dimensional object the interatomic distance is $d_v=2.24/(\rho_v)^{1/3}$ for a compact packing [33]. When using this three-dimensional relation for the shells, the interionic distance would decrease drastically at the $P(r)$ maximum. In our simulation, the expanding ionic shell constitutes a two-dimensional object. In this case the interatomic distance d_s is determined by the surface density ρ_s, namely $d_s=2.15/(\rho_s)^{1/2}$ for a compact packing [33]. The three-dimensional consideration is valid for $d_v \gg d_s$, whereas in the opposite case, $d_v \ll d_s$, the shell presents a monolayer and has to be treated as a two-dimensional sphere. It is interesting to inquire in what cluster size domain Coulomb explosion will generate a three-dimensional expanding shell. The ratio between these two interionic distance values is roughly expressed by the relation

$$d_v/d_s=1.04(\delta/4\pi)^{1/6}(\Delta R/R)^{1/3}n^{1/6}, \tag{22}$$

which is determined by the 1/3 power of the ratio of the shell width ΔR and the radius R, where according to our simulations the ratios $\Delta R/R$ attain a nearly constant value at longer times (Figs. 6, 7, and 9). n is the number of the cluster A ions, and δ is the fraction of ions located inside the shell. From our simulations for R_H and ΔR we infer that $d_v/d_s \sim 1$ for $n \approx 15\,000$ and consequently the expanding shells can be considered as being three-dimensional only for very large exploding clusters with $n \gg 15\,000$. For clusters consisting of $\sim 15\,000$ atoms or less, the apparent volume density $\rho_v=n\delta/V$, with V being the shell volume, does not constitute a meaningful concept for the characterization of the density. Consequently, the drastic increase of ρ_v in this size domain does not indicate any drastic decrease in the interionic distances and in the generation of shock waves in the Coulomb explosion of multicharged clusters in the size domain ($n \simeq 10^2-10^4$) considered herein. This conclusion is in contrast with the proposal and analysis of Kaplan *et al.* [32]. According to Eq. (22) it is possible to expect a real drastic decrease in the interionic distances and even in the generation of shock waves for $n \gg 15\,000$. However, the repulsion between shell ions, which is not taken into account by the electrostatic model of expansion presented above, will probably prevent the drastic increase in the density. The features of such a Coulomb exploding multicharged monolayer of light–heavy multicharged heteroclusters are qualitatively distinct for the uniform Coulomb explosion of homonuclear multicharged clusters [16], e.g., $(A^+)_n$.

Compelling experimental and theoretical evidence [4–6,18–22] was advanced for nuclear fusion driven by Coulomb explosion of deuterium containing homonuclear [4,5,9,11,16,22] and heteronuclear [6,11,19–22] clusters. Applications of Coulomb explosion of deuterium containing light–heavy atom heteroclusters, e.g., $(DI)_n$, in ultraintense laser fields will involve *dd* nuclear fusion driven by heterocluster Coulomb explosion [18] where the extremely charged I^{q+} $(q=7-35)$ ions act as most effective energetic and kinematic triggers for driving the expanding D^+ ions. The energetic triggering is manifested by the large value of $E_{av} \propto q_B$, according to Eqs. (6a) and (7a). Thus, e.g., for Coulomb explosions of the heteronuclear $(D^+I^{25+})_{2171}$ cluster, $E_{av} \simeq 23$ keV, while for Coulomb explosion of the first-row $(C^{+q}D_4^+)_{2171}$ heterocluster, $E_{av}=5.8$ keV [20,22]. This increase of the deuteron energy by a numerical factor of 3 in Coulomb explosion of the light–heavy $(DI)_n$ heterocluster will provide a 2–3 order of magnitude enhancement of the cross section for the *dd* fusion reaction and of the neutron yield, as compared to that for Coulomb explosion of the first-row $(CD_4)_n$ heterocluster of the same size. Furthermore, the kinematic effects manifested in the narrow kinetic energy distribution of the D^+ ions from Coulomb exploding light–heavy $(DI)_n$ clusters may be of advantage in a further increase of the nuclear fusion yield.

ACKNOWLEDGMENTS

The authors are grateful to Dr. Andreas Heidenreich for discussions, comments, and help with data representation. This research was supported by the Deutsche Forschungsgemeinschaft (Sfb 450) on "Analysis and Control of Ultrafast Photoinduced Reactions" and by the Binational German–Israeli James Franck Program on Laser–Matter Interaction.

[1] T. Ditmire, T. Donnelly, R. W. Falcone, and M. D. Perry, Phys. Rev. Lett. **75**, 3122 (1995).
[2] T. Ditmire, R. A. Smith, J. W. G. Tisch, and M. H. R. Hutchinson, Phys. Rev. Lett. **78**, 3121 (1987).
[3] T. Ditmire, J. W. G. Tisch, E. Springate, M. B. Mason, N. Hay, J. P. Marangos, and M. H. R. Hutchinson, Phys. Rev. Lett. **78**, 2732 (1997).
[4] T. Ditmire, J. W. G. Tisch, E. Springate, M. B. Mason, N. Hay, R. A. Smith, J. Marangos, and M. H. R. Hutchinson, Nature (London) **386**, 54 (1997).
[5] J. Zweiback, R. A. Smith, T. E. Cowan, G. Hays, K. B. Wharton, V. P. Yanovsky, and T. Ditmire, Phys. Rev. Lett. **84**, 2634 (2000).
[6] G. Grillon, Ph. Balcou, J.-P. Chambaret, D. Hulin, J. Martino, S. Moustaizis, L. Notebaert, M. Pittman, Th. Pussieux, A. Rousse, J.-Ph. Rousseau, S. Sebban, O. Sublemontier, and M. Schmidt, Phys. Rev. Lett. **89**, 065005 (2002).
[7] J. Schulz, H. Habnitz, T. Laarmann, S. Gürtler, W. Laasch, A. Swiderski, Th. Möller, and A. A. B. de Castro, Nucl. Instrum. Methods Phys. Res. A **507**, 572 (2003).
[8] V. Kumarappan, M. Krishnamurthy, and D. Mathur, Phys. Rev. A **67**, 063207 (2003).
[9] R. W. Madison, P. K. Patel, D. Price, A. Edens, M. Allen, T. E. Cowan, J. Zweiback, and T. Ditmire, Phys. Plasmas **11**, 270 (2004).
[10] T. Ditmire, Phys. Rev. A **57**, R4094 (1998).
[11] I. Last and J. Jortner, Phys. Rev. A **64**, 063201 (2001).
[12] I. Last and J. Jortner, Z. Phys. Chem. (Munich) **127**, 975 (2003).
[13] Ch. Siedschlag and J. M. Rost, Phys. Rev. A **67**, 013404 (2003).
[14] I. Last and J. Jortner, J. Chem. Phys. **120**, 1348 (2004).
[15] I. Last and J. Jortner, J. Chem. Phys. **120**, 1336 (2004).
[16] I. Last and J. Jortner, J. Chem. Phys. **121**, 3030 (2004).
[17] I. Last, I. Schek, and J. Jortner, J. Chem. Phys. **107**, 6685 (1997).
[18] V. P. Krainov and A. S. Roschchupkin, Phys. Rev. A **64**, 063204 (2001).
[19] I. Last and J. Jortner, Phys. Rev. Lett. **87**, 033401 (2001).
[20] I. Last and J. Jortner, J. Phys. Chem. A **106**, 10877 (2002).
[21] J. Jortner and I. Last, ChemPhysChem **3**, 845 (2002).
[22] I. Last and J. Jortner, J. Chem. Phys. **121**, 8329 (2004).
[23] I. Last and J. Jortner. Proc. Natl. Acad. Sci. U.S.A. **102**, 1291 (2005).
[24] D. A. Card, E. S. Wisniewski, D. E. Folmer, and A. W. Castleman Jr., J. Chem. Phys. **116**, 3554 (2002).
[25] V. P. Krainov and M. B. Smirnov, Phys. Rep. **370**, 237 (2002).
[26] I. Last and J. Jortner (unpublished).
[27] J. W. G. Tisch, N. Hay, E. Springate, E. T. Gumbrell, M. H. R. Hutchinson, and J. P. Marangos, Phys. Rev. A **60**, 3076 (1999).
[28] E. Springate, N. Hay, J. W. G. Tisch, M. B. Mason, T. Ditmire, M. H. R. Hutchinson, and J. P. Marangos, Phys. Rev. A **57**, 063201 (2000).
[29] F. Dorchies, F. Blasco, T. Caillaud, J. Stevefelt, C. Stenz, A. S. Boldarev, and V. A. Gasilov, Phys. Rev. A **68**, 023201 (2003).
[30] R. Bersohn and A. H. Zewail, Ber. Bunsenges. Phys. Chem. **92**, 373 (1988).
[31] K. Boyer, T. S. Luk, J. C. Solem, and C. K. Rhodes, Phys. Rev. A **39**, 1186 (1989).
[32] A. E. Kaplan, B. Y. Dubetsky, and P. L. Shkolnikov, Phys. Rev. Lett. **91**, 143401 (2003).
[33] R. Zallen, *The Physics of Amorphous Solids* (John Wiley, New York, 1983).